Fluorescence Ratio Imaging Microscopy: Temporal and Spatial Measurements of Cytoplasmic pH

Gary R. Bright, Gregory W. Fisher, Jadwiga Rogowska, and D. Lansing Taylor

Department of Biological Sciences, Center for Fluorescence Research in Biomedical Sciences, Carnegie-Mellon University, Pittsburgh, Pennsylvania 15213

Abstract. Fluorescence ratio imaging microscopy (Tanasugarn, L., P. McNeil, G. Reynolds, and D. L. Taylor, 1984, *J. Cell Biol.*, 98:717–724) has been used to measure the spatial variations in cytoplasmic pH of individual quiescent and nonquiescent Swiss 3T3 cells. Fundamental issues of ratio imaging that permit precise and accurate temporal and spatial measurements have been addressed including: excitation light levels, lamp operation, intracellular probe concentrations, methods of threshold selection, photobleaching, and spatial signal-to-noise ratio measurements. Subcellular measurements can be measured accurately (<3% coefficient of variation) in an area of 3.65 μm^2 with the present imaging system. Quiescent Swiss 3T3 cells have a measured cytoplasmic pH of 7.09 (0.01 SEM), whereas nonquiescent cells have a pH of 7.35 (0.01 SEM) in the presence of bicarbonate buffer. A unimodal distribution of mean cytoplasmic pH in both quiescent and nonquiescent cells was identified from populations of cells measured on a cell by cell basis. Therefore, unlike earlier studies based on cell population averages, it can be stated that cells in each population exhibit a narrow range of cytoplasmic pH. However, the mean cytoplasmic pH can change based on the physiological state of the cells. In addition, there appears to be little, if any, spatial variation in cytoplasmic pH in either quiescent or nonquiescent Swiss 3T3 cells. The pH within the nucleus was always the same as the surrounding cytoplasm. These values will serve as a reference point for investigating the role of temporal and spatial variations in cytoplasmic pH in a variety of cellular processes including growth control and cell movement.

THE cytoplasm of living cells is a highly organized and dynamic system of molecular interactions and chemical reactions (13, 32, 38, 71, 72). The precise spatial orchestration of these reactions leads to such cellular events as exocytosis, cell movement, cell division, chemotaxis, phagocytosis, and directed intracellular transport. Without some spatial component to the control and performance of these reactions, it is difficult to understand how such directed events could occur. Thus, an understanding of cell biology at the molecular level requires an understanding of how cells control and perform this spatial orchestration.

Quantitative fluorescence imaging microscopy has become a powerful tool in cell and molecular biology because it permits the measurement of both spatial and temporal dynamics of molecules and organelles in living cells (2, 69, 70–72). The roots of this technology extend to the early use of microspectrophotometry on both living and fixed cells (9, 55). The superior sensitivity, specificity, and spectroscopic capabilities of fluorescence microscopy encouraged the development of advanced detection systems (6, 14, 31, 53, 59, 63, 73, 83, 85), fluorescent probes and biologicals (see 82), and physical optical methods (see 36). The developments in fluorescence imaging microscopy have been rapid in the last few years (1–4, 6, 16, 29, 69, 84).

Unfortunately cells are not optimal "cuvettes" for spectroscopic studies. Several serious problems in quantifying optical signals from living cells arise due to variations in optical pathlength, local probe concentrations, light scattering, illumination intensity, and photobleaching. These variations exist within different regions of the same cell and from cell to cell in a population. Additionally, these parameters also vary in time within individual cells due to the dynamic nature of living cells. Most of these problems can be successfully overcome or minimized by measuring the ratio of absorbance (39, 75) or fluorescence (25, 52, 69) at two wavelengths.

Ratio spectroscopy requires that the probe be differentially sensitive to the parameter of interest in at least two absorption or emission wavelengths. The emission at one wavelength may be either nonsensitive (i.e., isosbestic point), much less sensitive, or sensitive in the opposite direction compared to the emission of the other wavelength. It is the relationship of the changes in emission or absorption at each wavelength with respect to each other that defines the measured response. Because the absorption or emission originates from the same specimen volume, the ratio relationship normalizes for optical pathlength, local probe concentration, illumination intensity, and photobleaching. Whole spectra

are not required since measurements at these two wavelengths reflect the spectral changes in response to the environment.

Specific fluorescent probes such as pH-sensitive fluorescein and calcium-sensitive Quin-2 or Fura-2 have been used to quantify a population average of these parameters using fluorometers (e.g. 10, 24, 47, 49, 52, 60, 75, 77). We extended the ratio method to the microscope and measured cytoplasmic pH (25, 26) and endosomal pH in single cells (27, 41; see also 78, 79) to validate the general approach. Subsequently, we demonstrated that similar results could be obtained by fluorescence imaging microscopy and by photomultiplier based microspectrofluorometry (69). Thus, a method was available for obtaining spatial, as well as temporal, spectroscopic information from single living cells. In addition, several other applications of ratio imaging were also proposed including the spatial quantitation of other physiological parameters, local relative concentrations of fluorescent analogs, resonance energy transfer and polarization of fluorescence (69). Recently, the ratio imaging approach has been applied to measurements of cellular pCa using fluorescent indicators of calcium (30, 33, 54, 57, 65, 86). A ratio spectroscopic approach has also been applied in flow cytometry (49).

There is enormous potential for using ratio imaging techniques to map physiological parameters, the specific distribution of molecules, and the molecular activity of specific molecules in living cells (72). However, there are important aspects of a fluorescence imaging microscope system that must be considered before the methodology can yield reliable results. These include: low light level cameras used as radiometric devices; maintenance of cellular physiology on the microscope stage; and image processing and analysis methods applied to quantitation of spatial information. The present paper will address some of these technical issues applicable to any ratio imaging experiment, while focusing on the measurement of cytoplasmic pH.

Cytoplasmic pH has been implicated in a variety of cellular regulatory processes (7, 8; see also 5, 51). Cytoplasmic pH influences the free calcium ion concentration and the activity of certain structural proteins and enzymes (8). Therefore, a precise and accurate measurement of the cytoplasmic pH in individual cells is necessary to interpret temporal and spatial variations in all cellular chemical processes. The present paper aims to define the cytoplasmic pH of individual Swiss 3T3 cells in two extreme states: cells cycling through the cell cycle in the presence of serum; and quiescent cells (G_0) arrested by serum starvation. Furthermore, the existence of spatial variations in cellular pH is investigated. These values will serve as a reference point for investigating the role of cytoplasmic pH in a variety of cellular processes including growth control and cell movement (see 40 for a recent review).

Materials and Methods

Preparation of Cells. Swiss 3T3 cells (No. CCL92; American Type Culture Collection, Rockwell, MD) were grown in Dulbecco's modified essential medium (DMEM) without phenol red (GIBCO, Grand Island, NY), supplemented with 0.3 mg/ml L-glutamine, 50 U/ml penicillin, 0.05 mg/ml streptomycin, and 24 mM sodium bicarbonate, pH 7.4 (bDMEM), plus 10% calf serum (cDMEM). Cells were maintained in logarithmic growth at 37°C in 5% CO_2. Passage numbers ranged from 116 to 124. Cells were used no more than 4–5 wk. All media used in the microscope culture chamber were preequilibrated at least 48 h in a culture incubator at 37°C, 5% CO_2.

Fluorescent Probes. Fluorecein-labeled dextran (70,000 D; FD[1] (FD-70S; Sigma Chemical Co., St. Louis, MO) was dialyzed against 50 mM KCl and 10 mM Tris, pH 8, and fractionated on a 4 × 100-cm column (Sephacryl S-300; Pharmacia Fine Chemicals, Piscataway, NJ) in the same buffer at 4°C. The center 80% of the large fluorescent peak was pooled, exhaustively dialyzed against water, and lyophilized. 2.7'-bis (2-carboxyethyl)-5,6-carboxyfluorescein (BCECF) and the cell permeant acetoxymethyl ester derivative (BCECF-AM) were purchased from Molecular Probes, Inc. (Eugene, OR). BCECF-AM was dissolved in dry DMSO at a concentration of 2 mM and stored at −20°C. BCECF was dissolved in water and stored at −20°C.

Preparation of Fluorescently Labeled Cells. Cells in a 100-mm culture dish were scrape loaded (41) with 0.45 ml of 13 mg/ml fluorescein dextran. The scrape-loading buffer was 150 mM KCl, and 5 mM Hepes, pH 7.4. Cells were washed once and plated onto 40-mm coverslips (Bellco Glass, Inc., Vineland, NJ) in 100-mm culture dishes. This was conveniently done by placing a dry sterile coverslip into a 100-mm dish. Cells (50–100 μl) were added to the center two-thirds of the coverslip to give a cell density as high as possible yet maintaining predominantly single cells after spreading. After a 2–5-h recovery in cDMEM the plates were washed and 10–15 ml of bDMEM (starved) or cDMEM (nonstarved) added. Cells were then incubated for 18–24 h. This approach provides sufficient culture medium for mounting the cells in the microscope cell chamber, thus minimizing alterations in the cell environment.

Cells used for BCECF-AM–labeling were harvested and plated by scrape loading in the presence of buffer alone or by trypsinization and treated as above. Before observation, cells were labeled in a 60-mm dish with 4 ml 2.5 μM BCECF-AM in Hank's balanced salt solution in a culture incubator for 5–7 min (starved) or 30–45 min (nonstarved). Coverslips were washed three times and returned to the original 100-mm dishes. After at least 30-min recovery in the incubator, cells were mounted on the microscope stage and allowed to equilibrate until the temperature stabilized at 37°C (5–10 min). In all cases, the cells recovered and were mounted in the microscope culture chamber in the culture medium from the original 100-mm plate.

Standard Curves. Both in vitro and in situ standard curves were made using 130 mM KCl, 1 mM $MgCl_2$, 15 mM MES, and 15 mM Hepes. The pH was adjusted appropriately with KOH. In vitro standard solutions included FD or 10 μM BCECF. In vitro standard curves were produced using a chamber made with a microscope slide (Clay Adams Divisio Parsippany, NJ), a silicone rubber gasket (Millipore Swinnex-25, Millipore/Continental Water Systems, Bedford, MA), and a 25-mm diam coverslip. The gasket was lightly greased with high vacuum silicone grease, sealing the solution between the coverslip and the slide.

In situ standard curves were prepared using the standard curve buffer solution with the addition of 10 μg/ml nigericin (Sigma Chemical Co.) from a 10 mg/ml stock solution in 100% ethanol, stored at −20°C (75). The nigericin was added just before use. 10 ml of each buffer were prepared and loaded into 10-ml syringes and placed in a tissue culture incubator at 37°C. Labeled cells were mounted onto the microscope stage and the chamber was perfused with 10 ml of the appropriate buffer. The cells were incubated with the first solution for at least 5–10 min to allow complete equilibration before recording data. Subsequent solutions required <1 min for equilibration.

Fluorescence Recovery after Photobleaching. Fluorescence recovery after photobleaching (FRAP) was performed according to Luby-Phelps et al. (37, 38).

Fluorescence Ratio Imaging Microscope System

Microscope Cell Chamber. The culture chamber used in these studies was a modified Sykes-Moore chamber. The conventional Sykes-Moore chamber (51 mm diameter; Bellco Glass, Inc.) used a rubber O-ring as a spacer. This was replaced by a stainless steel ring with three 18-gauge needles, silver-soldered in place, that provided access to the inside of the chamber. A stainless steel baffle was soldered across the entrance port to disperse the fluid flow into a broad stream. Thin latex rubber gaskets (made from dental dam) were used to seal the chamber. A thermistor (10,000 ohm, 0.014-inch diam;

1. *Abbreviations used in this paper*: BCECF, 2', 7'-bis-(2-carboxyethyl)-5(and 6-)carboxyfluorescein; BCECF-AM, acetoxymethyl ester of BCECF; CV, coefficient of variation; FD, fluorescein-labeled 70,000-D dextran; FRAP, fluorescence recovery after photobleaching; Im^{489}, IM^{452}, image recorded using 489- or 452-nm excitation of light; S/N, signal to noise ratio.

Thermometrics, Inc., Edison, NJ) was inserted through one needle into the chamber and the needle was sealed with plasticine. External pH was monitored with a flow-through electrode (Markson Science Inc., Phoenix, AZ) when continuous perfusion was used. The pH of the culture fluid was always recorded before mounting cells into the chamber using a standard pH meter and electrode. The pCO_2 was not measured directly but was presumed constant since the medium pH was constant. This closed cell chamber used with medium preequilibrated with CO_2 eliminated the need for organic buffers.

Temperature control was provided by two systems. Coarse control was provided by a custom heating stage designed around the Sykes-Moore chamber by Rainin Instrument Co., Inc. (Boston, MA). The Rainin heating unit was adjusted to provide 95% of the heat necessary to maintain 37°C. The second system for fine temperature stabilization, consisted of a modified air curtain (Sage Instruments, Div. Orion Research, Inc., Cambridge, MA) wired for feedback control by a microprocessor (MEK6802D5; Motorola Semiconductor Group, Phoenix, AZ) that measured and displayed the output from the thermistor placed in the culture chamber. The culture fluid was maintained at 37°C ± 0.2°C.

Imaging System. The ratio imaging system is a significant extension of the one described previously (69). The optical system is based on a Zeiss Universal microscope stand with several modifications to the excitation light path: (*a*) A 12-V tungsten-halogen filament lamp in a standard Zeiss lamp housing was operated at 8 A using a power supply (model JQE 15-12M; Kepco, Inc., Flushing, NY) set up to operate in constant current mode. This power supply isolated the lamp from line voltage fluctuations. Monitoring lamp output with a power meter (Newport Corp., Fountain Valley, CA) indicated a very stable light level. (*b*) An electromechanical shutter (Uniblitz, 225L2AOX5; Vincent Associates, Rochester, NY) was mounted immediately in front of the lamp housing and provided control over the excitation light exposure. (*c*) A two-position aluminum filter holder (see 69) mounted on a stepper motor (Slo-syn MO-61; The Superior Electric Co., Bristol, CT) with custom interference filters (452-, 489-, and 10-nm bandpass. Spectro-Film, Inc., Winchester, MA), was placed immediately in front of the standard Zeiss epi-condenser. The excitation light levels at 489 nm and 452 nm were adjusted, using neutral density filters, such that emission ratios were >1 in the pH range of interest.

The emission light path included a standard Zeiss narrow band fluorescein barrier filter and dichroic reflector with a Plan-Neofluar 63×, oil immersion objective (1.25 NA; Carl Zeiss, Inc., Thornwood, NY). Images were recorded with a Dage-MTI ISIT camera operated in manual mode. The intensifier was operated at 9,000 V and the gain set to 20% of the maximum setting, providing the best image based on sensitivity and contrast (6). All quantitative data was recorded within the center 50% of the field which had <5% shading error. This amount of shading had no significant effect on the measurement of the mean ratio. Therefore a whole field shading correction was not required. At these camera settings the center 50% of the field had a linear radiometric response.

The microscope culture chamber and Rainin heating unit were mounted on a Zeiss scanning stage (0.5 μm step size). The stage coupled to the peripherals controller provided the ability to record the coordinates of large numbers of cells and to repeatably locate these cells. Once the coordinates of the cells had been recorded within the memory of the peripherals controller, each could be recalled on demand by the user or by the image processor.

A custom peripherals controller was used to coordinate control of the shutter, filter changer, and scanning stage. The controller was constructed using a Motorola 68000 single-board computer (model MEX68KECB; Motorola Microsystems, Phoenix, AZ). Assembly language programs controlled the peripherals through a parallel port at the direction of the user or the image processor. This system executed the sequence of opening and closing the excitation shutter, changing the filters, and finding a series of cells whose coordinates had been previously stored. The sequence used in this study was: (*a*) find the next cell; (*b*) set 489-nm filter in place; (*c*) open shutter to allow focus; (*d*) image processor integrates image; (*e*) set 452-nm filter in place; (*f*) image processor integrates image; (*g*) close shutter. All manipulations occur automatically except for focusing.

Image Processing and Analysis. Images were recorded with an image processor (VDP 1800; VICOM Systems, Inc., Junction City, CA) averaging 128 video frames. After background subtraction, a threshold level was determined interactively for each cell. The threshold was determined for the image recorded at 452 nm because it had the lower signal-to-noise ratio (S/N). Cells labeled with FD exhibited variable numbers of presumed autophagic vesicles. These vesicles showed a very high concentration of probe and were especially obvious in the image recorded at 452 nm. An upper threshold value was set to exclude the vesicles from subsequent calculations. The mean ratio within the mask defined by the threshold was calculated on a pixel by pixel basis using floating point operations with a program written in PASCAL. Subsequent statistical data analysis was performed with DATAPLOT (National Bureau of Standards, available from National Technical Information Service, Springfield, VA) on a computer (VAX 11/750; Digital Equipment Corp., Maynard, MA). We have used floating point operations to generate the ratio values since this approach yields the most accurate results. An evaluation of other approaches will be discussed elsewhere (manuscript in preparation).

Spatial Analysis of Images. A solution of BCECF was used to determine the limits of the spatial S/N of the system, since a uniform solution should show no spatial variation. The usable region of the field (center 50%) was sampled with 60 uniformly distributed nonoverlapping areas. The sampling areas varied from 0.074 (1 pixel, 0.31 × 0.24 μm) to 71.6 μm^2 (31 × 31 pixels). The dimensions of an individual pixel were determined with a stage micrometer (Ealing Corp., South Natick, MA). Each sampling area, larger than one pixel, was represented by the mean of the pixels defining the area. The mean of the region is defined as the mean value of all the sampling areas described above. The coefficient of variation (CV) of these points was used as a measure of the spatial S/N.

A visual indication of spatial variation before and after spatial averaging was accomplished by creating an error map calculated according to:

$$|\text{image } (x,y)| = \frac{\text{pixel } (x,y) - \text{mean of region}}{\text{mean of region}} * 100$$

The image represents the difference (% error) that each pixel varies from the mean value. The degree of variation in an area is represented by the relative amount of "speckle" in the image. The magnitude of the variation is more readily observed in pseudocolor displays. When an error map of a cell is produced the mean of region is redefined as the mean ratio calculated within the mask.

Results

Validation of the Fluorescence Ratio Imaging Microscope

We have designed and constructed an improved imaging system for quantitative analyses of ratios of fluorescent signals from living cells. Experiments were performed to define the capabilities of the present instrument, as well as to further verify the concept of ratio imaging. Although ratios of images taken at two wavelengths can, in principle, be used to normalize variations in optical pathlength, local probe concentration, illumination intensity, photobleaching, and minimize effects of light scatter over a wide range of conditions (25–27, 69), it is still possible that experimental conditions can vary to such an extreme that ratioing can no longer normalize the data adequately. In terms of the imaging system, such conditions could result from factors that degrade the images and dramatically reduce their S/N. Therefore, we systematically studied the effects of a number of parameters that we felt were most likely to influence the performance of the fluorescence ratio imaging system. These included excitation light levels, lamp current, intracellular probe concentration, and methods for selecting thresholds before calculating the ratio. The effects of varying focus and photobleaching were also studied. The validation experiments used cells labeled with either BCECF-AM or FD and clamped to a pH of 6.98.

Light Level. The effect of varying intensity of the excitation light was studied by inserting a series of neutral density filters (Carl Zeiss, Inc.) into the excitation light path. Fig. 1 illustrates that attenuation of the excitation light over the range of 0–90% resulted in no significant change in the mean ratio values for cells clamped at pH 6.98. The lower and upper limits in excitation light levels were set by camera noise

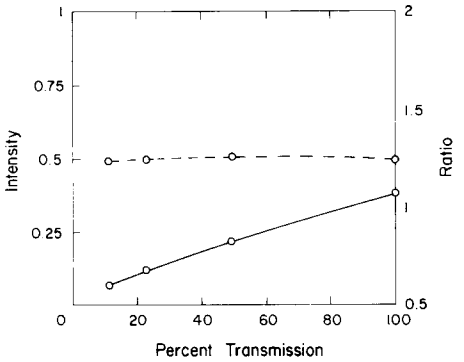

Figure 1. Effects of varying excitation light levels on the ratio. The pH of a single cell labeled with BCECF was clamped to 6.98. The excitation light was attenuated with a series of neutral density filters. Solid lines indicate changes in emission intensity using 489-nm excitation. Broken lines show the mean ratios.

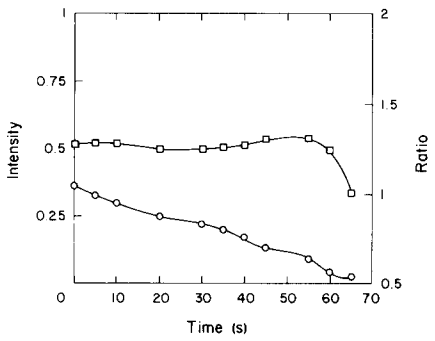

Figure 2. Effects of photobleaching on the ratio. The pH of a single cell labeled with BCECF was clamped to 6.98. The cell was exposed to constant illumination at 489 nm. At periodic intervals images were recorded for the calculation of the ratio. Circles indicate the emission intensity at 489-nm excitation. Squares indicate the mean ratio.

level and camera saturation, respectively. Thus, pH can be determined over a wide range of excitation light levels. Typically, the excitation light levels used were $\sim 1.78 \times 10^{-4}$ $\mu W/\mu m^2$ or less. Cellular autofluorescence and scattered light were not detectable at the excitation light levels and camera settings used.

Photobleaching. The effects of bleaching the probe on the ratio was assessed by continuously exposing cells to excitation at 489 nm. At periodic intervals images were recorded using 489-nm excitation (Im^{489}) and 452-nm excitation (Im^{452}) for calculation of the ratio. Continuous exposure resulted in a dramatic decrease in the fluorescence intensity over time (Fig. 2). However, the mean ratio remained relatively constant until the signal level decreased into the noise. This result demonstrated that even extensive photobleaching is normalized by the ratio measurement.

The procedure for acquiring pairs of experimental images utilized a sequence of exposing the cells to illumination at each wavelength for only the time required for integration (128 frames at each wavelength, ~4.5 s) to minimize photobleaching. In practice, there was no appreciable photobleaching at the irradiance used in these studies as indicated by the fact that changing the sequence of image acquisition from Im^{489}, Im^{452} to Im^{452}, Im^{489} did not alter the raw or ratio values. The absence of an effect of photobleaching on the ratio would be important for long term studies on cells involving multiple measurements. Specific experimental conditions will determine the balance between irradiance at the specimen plane and an acceptable S/N.

Lamp Current. The ratio values were not constant with respect to the operating current of the tungsten lamp (Fig. 3) as expected from the resulting change in the lamp color temperature (see 67). The steepness of the change confirmed the need for a highly regulated power supply with the lamp maintained at a constant current. We also noted that the color temperature changed with the age of the lamp. This latter observation was most evident by comparing standard curves taken at intervals of more than 3 wk. Good reproducibility was attained by using standard curves and experimental data collected within a period of 2 wk or less. Daily evaluation of the lamp was determined by measuring the mean ratio of cells clamped to a specific pH.

Focus. The image represents a two-dimensional projection of a three-dimensional cell. Thus, the image includes both in focus and out of focus components. The effect of focus on the ratio measurement was determined by calculating the mean ratio of a cell at various degrees of over and under focus. The mean ratio was constant, within ~3% error, for 3 μm over or under focus. Thus, slight changes in focus did not significantly affect the measured mean values. Nonclamped cells also did not exhibit changes in the ratio with focus.

Probe Concentration. Cells were labeled with BCECF and FD to various levels and the ratios were calculated. High levels of labeling were accommodated by placing neutral density filters in the excitation light path to bring the emission intensity within the dynamic range of the camera. All levels of labeling that were nontoxic to the cells gave similar ratio values. No inner filter effects have been detected over the range of probe concentrations used. In practice the minimum amount of probe giving a suitable S/N was used.

Threshold. The measurement of the mean cytoplasmic pH of a single cell in an image requires a threshold operation to separate the cell from the background. In this study all thresholds were determined interactively. To assess the effectiveness of the interactive approach to determining a threshold value, pH-clamped cells were used as models. A series of narrow masks were created by selecting lower and upper threshold values that divided the intensity range of the Im^{452} into seven levels. The lowest and highest threshold values generally represented the thin peripheral edges and the thick nuclear regions, respectively. The ratio at the edge of the cell should be the same as that at the center in pH-clamped cells. Fig. 4 illustrates that the mean ratios were similar for all

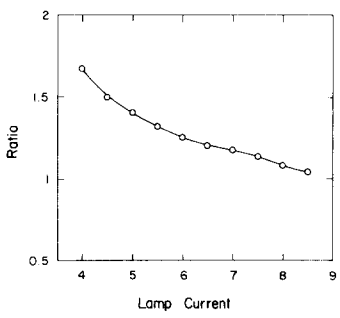

Figure 3. Effects of the operating current of a tungsten lamp on the ratio. The mean ratio of a pH-clamped cell was determined at each lamp current setting.

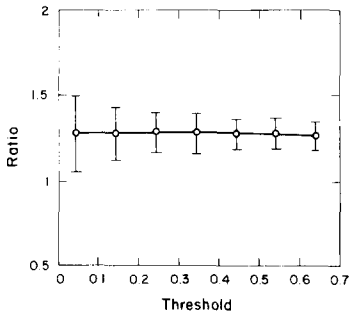

Figure 4. Effects of threshold value selection on the ratio. The Im^{452} of a single pH-clamped cell was divided into seven intensity levels. The mean and sample standard deviation of the ratio image was calculated for each level. The lower threshold value of each level is plotted on the *x* axis.

regions from the center to the edge of the cell. If the threshold value was too low and included regions with low S/N, the ratio value at the edge would deviate significantly from the ratio at the center. In practice, the threshold values were determined conservatively to avoid complications at the very edge of the cell. The figure also illustrates the decrease in the S/N (i.e., increase in CV) in the thin periphery of the cell as opposed to the center of the cell. Threshold values for Figs. 6 and 11 were chosen more liberally for presentation purposes.

Cell locomotion during the time of recording Im^{489} and Im^{452} could result in displacement of the images that would invalidate the ratio. This was never a problem in pH-clamped cells since they did not move. Even in the case of untreated Swiss 3T3 cells, locomotion was so slow that movement of this kind rarely influenced the ratio values. However, subcellular movements such as ruffling, vesicle movement, and nuclear movement could complicate the ratio in local regions, putting the ratio of that region into question (see Figs. 6 and 7 *b*).

Standard Curves

Accurate standard curves must be established to translate ratio values into pH values. Fig. 5 illustrates in situ standard curves for both BCECF and FD. The measured pKa of BCECF was 6.99 (0.03 SEM) and the useful range was pH 6.4–7.4. Rink et al. (60) reported a pKa of 6.97. FD had a measured pKa of 6.33 (0.04 SEM) and a range of 5.7–6.75, while the reported pKa is 6.2–6.5 (20, 52). We have focused our attention on BCECF as a probe of cytoplasmic pH due to the more suitable pKa.

The cells often increased in volume and formed large blebs after 20–40 min of incubation in nigericin as would be predicted from such an ionic manipulation of cells (see 89). However, ratio measurements before and after formation of any blebs always gave the same values. The bleb formation was minimized if the acidic solutions were used first.

Cell Labeling and Viability

Fluorescein Dextran. Nonspecific proteins (25–27) and then dextrans (18, 64, 69) have been used as carriers of pH indicators to limit the penetration of the indicator into selected compartments and to avoid nonspecific binding of the indicator to cellular components (37, 38). The effects of loading cells with fluorescein-labeled dextrans via scrape loading has previously been assessed and the cells exhibit no signs of toxicity (42–44). Cells can be monitored for long periods of time, limited only by dilution of the probe due to cell division and relatively slow autophagocytosis.

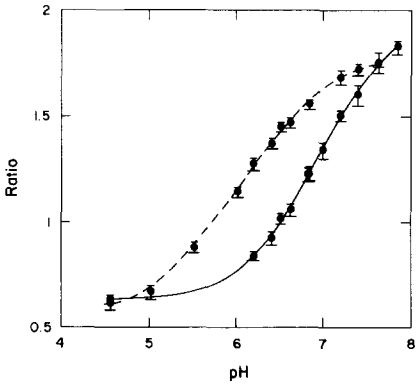

Figure 5. In situ standard curves for FD and BCECF. Each point represents the mean and sample standard deviation of the ratio for 10 cells. The measured pKa of FD (*broken line*) is 6.33 and BCECF (*solid line*) is 6.99.

Cells labeled with FD were allowed to recover in cDMEM before serum starvation. Cells serum starved for 24 h exhibited numerous fluorescent vesicles primarily in the perinuclear region and showed low ratio values indicating a low pH. This observation was consistent with the low pH found in endosomes (21, 26, 41, 49, 52, 69, 78), as well as the increased activity of lysosomal degradation pathways found in serum-starved cells (23). The vesicles could be removed by choosing an upper threshold value in addition to the lower threshold before performing the ratio calculation. Fig. 6 presents the ratio image of a cell illustrating the presence of vesicles with a pH clearly lower than the surrounding cytoplasm. Cells maintained with serum exhibited very few such vesicles and did so only after several hours of incubation.

The fluorescence image recorded with excitation at either wavelength was dominated by the nuclear region of the cell when labeled dextrans of lower molecular weight were used since they filled the full volume of the cell including the nucleus (data not shown, see 38). Very large signals from the nuclear region limited the S/N attainable for the smaller signals usually at the cell periphery since the entire intensity range of the specimen must be within the dynamic range of the camera. The advantage of using a carrier molecule that does not penetrate the nucleus (Fig. 7 *a*) is twofold: (*a*) the more peripheral, primarily cytoplasmic regions of the cell dominate the image and a higher S/N is attainable for these regions; and (*b*) restriction of the probe to the cytoplasm, the compartment of interest simplifies the interpretation of the ratios. Although 70,000-D FD did not penetrate the pores of the nucleus, it also did not penetrate to the very peripheral edges of the cell as well as smaller molecules (see BCECF). This made imaging these regions more difficult (Fig. 7 *b*). Therefore, a range of carrier molecule sizes should be used in separate experiments to optimize for both S/N and spatial detection.

Fluorescence recovery after photobleaching (FRAP) demonstrated that 70,000-D FD used in this study existed as a single mobile species in the cytoplasm. There was no evidence of binding to cytoplasmic constituents (37, 38).

BCECF. Starved and nonstarved cells showed differential rates of labeling with BCECF-AM. To label both types of cell populations to approximately the same extent, starved cells

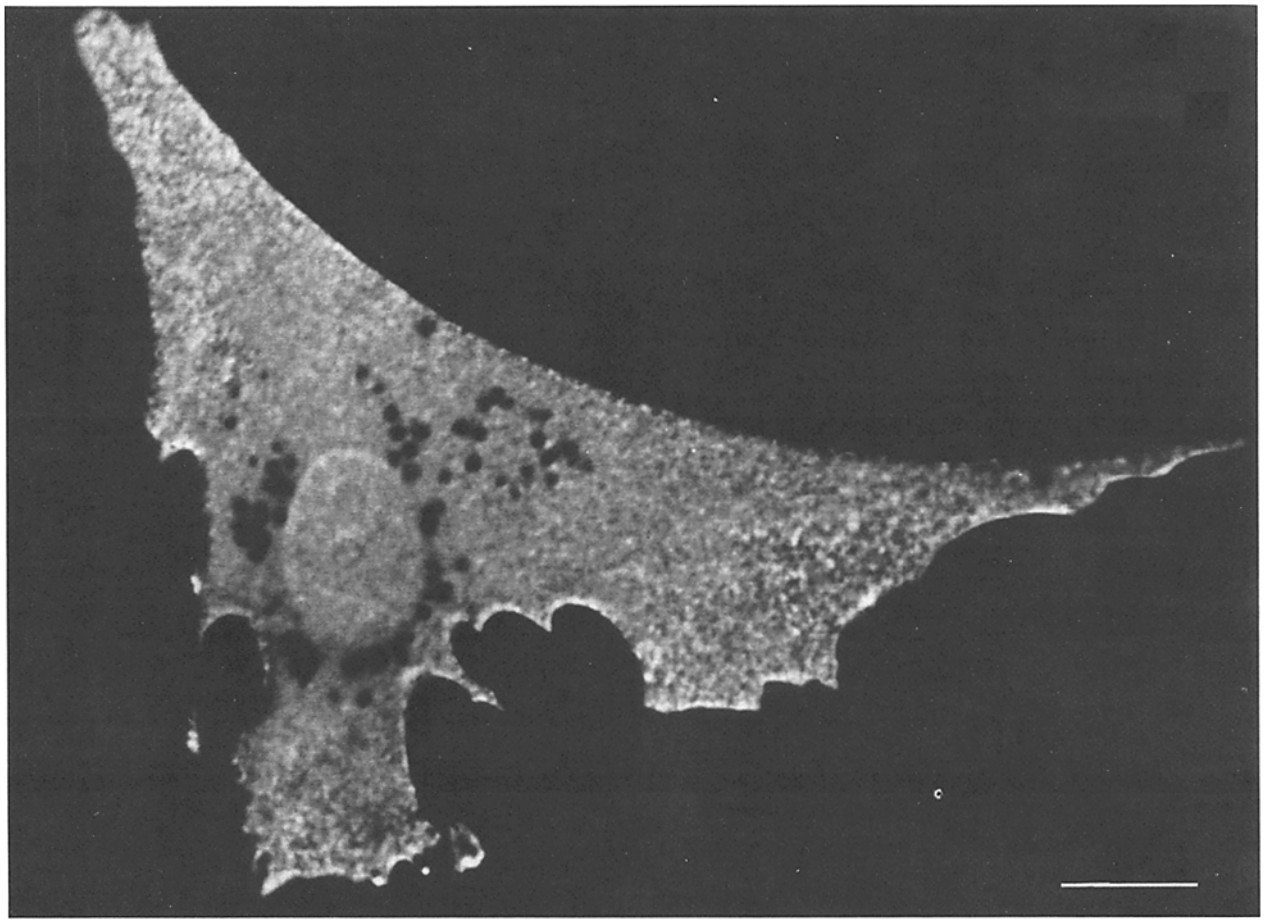

Figure 6. Ratio image of FD-labeled cell illustrates presence of nuclear, vesicular, and cytoplasmic subcellular compartments. The nucleus is visible due to a slight translation between the Im^{489} and Im^{452}. No difference in pH has been detected between the cytoplasm and nucleus. The acidic vesicles represent autophagosomes. Bar, 8 μm.

were incubated for 5–7 min while nonstarved cells were incubated for 30–45 min in 2.5 μM BCECF. Serum starvation apparently increased the cytoplasmic esterase concentration and/or activity. Numerous blebs appeared on cells immediately after labeling and required at least 30 min of incubation for recovery in the absence of BCECF-AM. This perturbation of the cells was observed for all labeling protocols tested. The present labeling scheme exhibited the most reproducible and least toxic effects.

The potential toxic effects of using the acetoxymethyl ester of BCECF, as well as the use of the microscope cell chamber, were assessed in a side by side comparison of populations of stained and unstained cells maintained in a 37°C incubator, and stained cells maintained at 37°C in the microscope cell chamber mounted on the microscope stage. There were no significant differences among the cell populations in terms of morphology (based on phase contrast microscopy) or vital dye (propidium iodide, trypan blue) exclusion for at least 3.5 h after recovery from labeling with BCECF. There was ~20% leakage of BCECF from nonstarved cells over a 2-h period. However, there was a significant loss of BCECF from ~50% of the cells, ~3 h after labeling the cells. This loss was abrupt and almost complete indicating potential long term effects of the dye on the physiology of the cells. Measurements of single cells followed throughout a 2-h period showed no change in the mean ratio.

BCECF is a small molecule that readily penetrates the pores of the nuclear membrane, as well as the most peripheral edges of the cell (Fig. 7, *c* and *d*). Potential complications of introducing small dye molecules such as BCECF-AM into cells include binding to cellular constituents and leakage into noncytoplasmic compartments in the cell. The absorbance spectrum of BCECF has been reported to shift 5 nm to the red after introduction into cells (60). If the dye molecule is adsorbing to cellular components or entering a subcellular compartment, the diffusion of the dye should be hindered. We have used FRAP to assess the mobility of the probe in different regions of the cell after different periods of incubation. We have been unable to detect any restricted mobility of the intracellular BCECF within 2-h postlabeling using the labeling protocol described above.

Spatial Analysis of Ratio Images

Fig. 6 shows the ratio image of a FD-labeled cell with obvious vesicular, nuclear, and cytoplasmic compartments. The vesicles exhibited a low pH that is consistent with a compartment due to autophagocytosis. The nuclear outline is clearly discernable in this cell. This illustrates one of the few times when the nucleus moved slightly between Im^{489} and Im^{452} acquisition. The average ratios inside and outside of the nucleus were always the same.

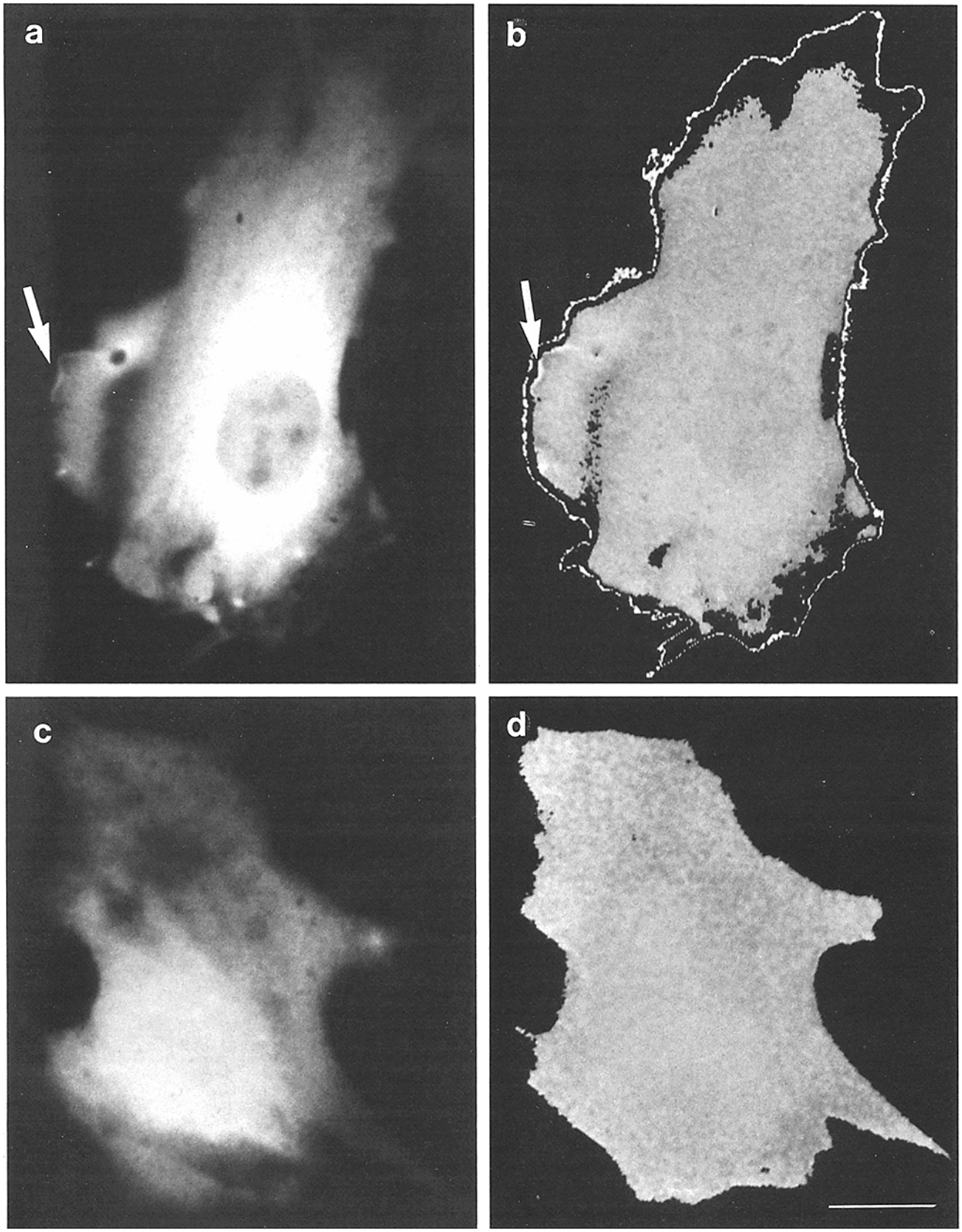

Figure 7. Comparison of cells labeled with FD and BCECF. FD-labeled cell (*a* and *b*) shows exclusion of the probe from the nucleus and limited penetration to the very peripheral edges of the cell. The outline in *b* defines the edge of the cell. The arrow illustrates an area of ruffling activity that results in the local misalignment of the Im^{489} and Im^{452}. The high resultant ratios are, therefore, meaningless in this local region. (*a*) Im^{489}; (*b*) ratio. BCECF-labeled cell (*c* and *d*) shows penetration of the probe throughout the volume of the cell, including the very peripheral edges. A large dynamic range is needed to image both the thick nuclear region and the thin peripheral edges of the cell. (*c*) Im^{489}; (*d*) ratio. Bar, 9 μm.

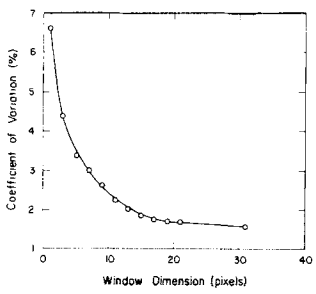

Figure 8. Relationship between spatial sample size and S/N. A solution of BCECF with a pH of 6.9 was used as an ideal specimen. A series of 60 sample areas were placed uniformly over the usable area of the field. Each area varied in size from 1 pixel (0.074 μm^2) to 31 × 31 pixel (71.6 μm^2) areas. The sample variance is used as a measure of the S/N.

One of the main purposes of applying a ratio imaging approach to measure physiological parameters is to detect spatial variations, as well as temporal changes, in living cells. The use of intensified cameras for low light level imaging dictates that certain trade-offs be made. One particular trade-off is between level of intensification and an adequate S/N (6, 69). In the current sytem each pixel represents a 0.31 by 0.24 μm area (0.074 μm^2). The spatial S/N of the imaging system, however, ultimately limits the spatial resolution of the measurements.

Fig. 8 shows the effect of the sampling area size on the ability to obtain a reliable ratio value in a uniform solution of BCECF. That is, what area (pixel dimensions) must be averaged to obtain a good measure of the ratio? A solution model represents an ideal specimen and should exhibit no spatial variation. Fig. 8 shows that an area of at least 3.65 μm^2 (7 × 7 pixels) must be averaged to reduce the CV to 3% using 10 μM BCECF. This concentration of BCECF results in a signal level similar to the level from BCECF-stained cells.

Fig. 9 shows a visual illustration of the improvement in spatial S/N after spatial averaging. Fig. 9 *a* shows the ratio image of a solution of BCECF. Fig. 9, *b* and *c*, represent error maps for the ratio image with no spatial averaging and averaging of 7 × 7 pixel regions (i.e., low pass filtering). There is a dramatic reduction in the spatial variation after spatial averaging. Therefore, with the present system, subcellular measurements can be measured accurately (<3% CV) in an area of ~3.65 μm^2.

The existence of a spatial variation of pH within a cell may be indicated by comparing the intracellular distribution of ratio values before and after clamping the pH with nigericin. Since the clamped cell should show no spatial variations in pH, a histogram of the pixel intensities should exhibit a narrow distribution around the mean value. Any deviation from this distribution in nonclamped cells may indicate the existence of two-dimensional variations in pH. Fig. 10, *a* and *c*, shows the histograms of the ratio values in a pH-clamped cell (*a*) and the same cell before clamping the pH (*c*). The distribution of ratio values within the cell is very narrow in both cases, and the distribution for the clamped cell appears to be symmetric as expected. The distribution in the nonclamped case is weakly skewed. However, visually, no obvious spatial variations in pH have been detected using enhancement techniques, such as pseudocolor displays. Thus, any spatial variations in pH are small in area.

Another method for potentially demonstrating spatial variations is the application of the error map. A pH-clamped cell should exhibit no spatial variations in pH and the error map should, therefore, show only spatial differences in S/N. In a nonclamped cell, any spatial variations in pH will be su-

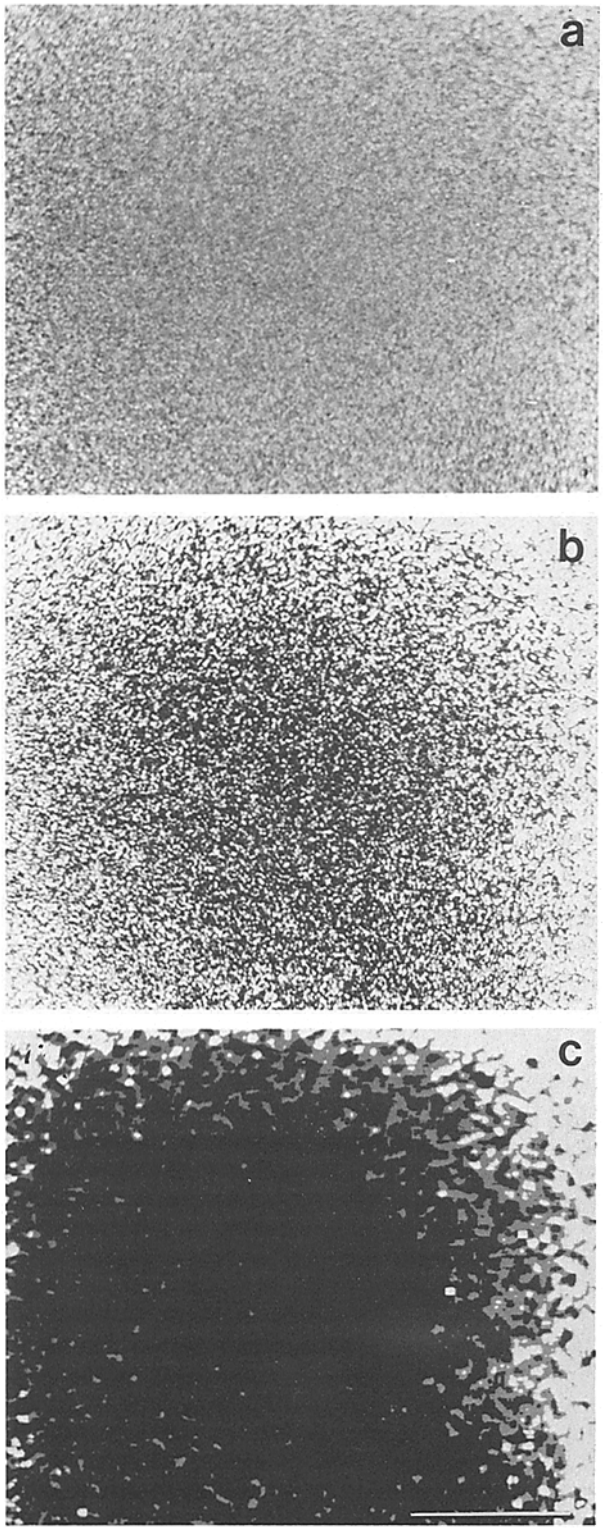

Figure 9. Visual illustration of spatial S/N using a solution of BCECF. A solution (10 μm^2) was used as an ideal specimen showing no spatial variation. An error map (see Material and Methods) was derived from (*a*) the ratio image with (*b*) no spatial averaging (1 pixel area, 0.074 μm^2) and (*c*) with 7 × 7 pixel averaging (3.65 μm^2). Bar, 20 μm.

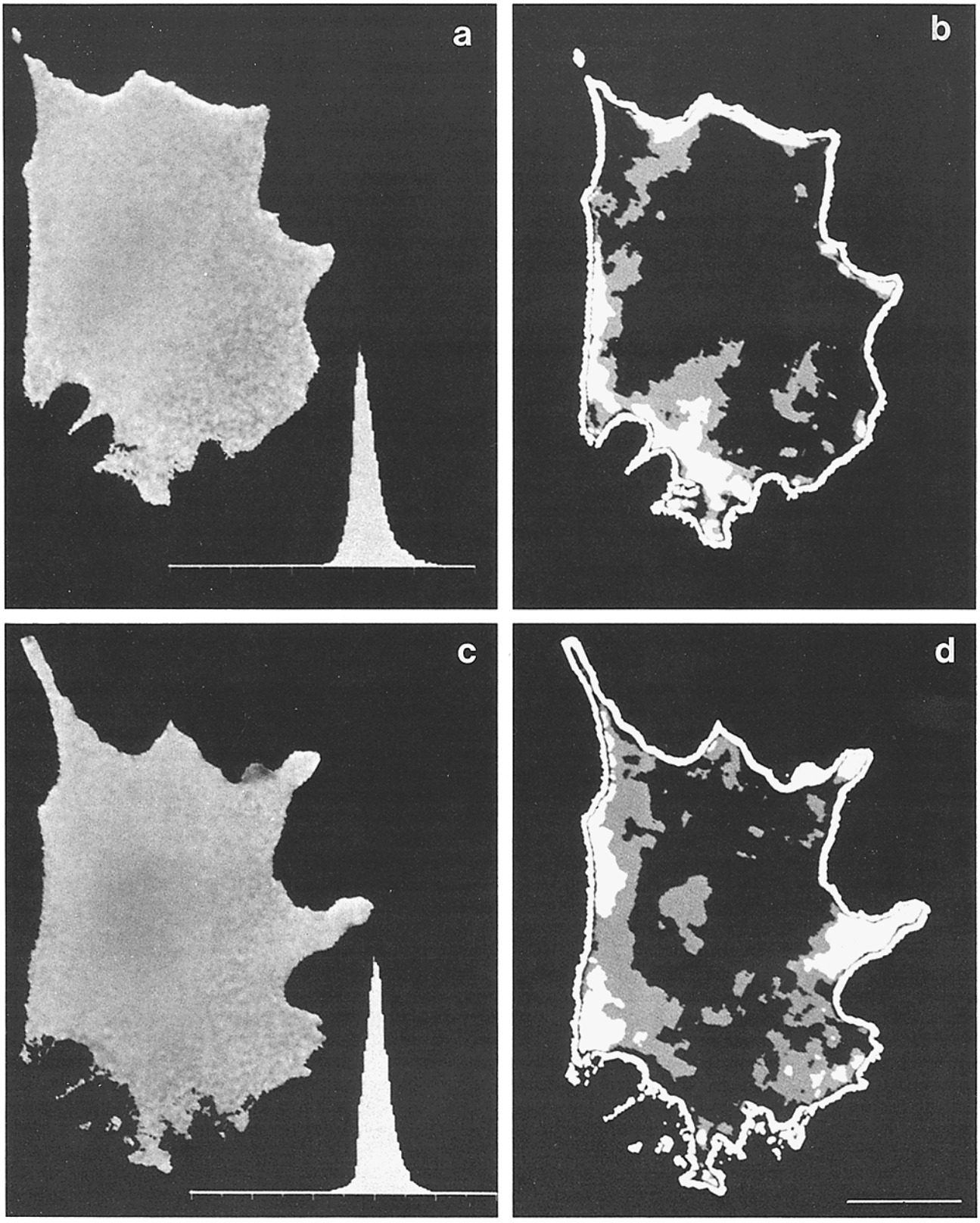

Figure 10. Distribution of ratio values inside a single cell before and after clamping pH. The histogram of ratio values in a pH-clamped cell (*a*) shows a narrow and approximately normal distribution, whereas, the same cell before clamping (*c*) shows a slightly skewed distribution. Error maps of these same images (*b* and *d*) show spatial variations that can be most easily explained by variations in S/N. Bar, 9 μm.

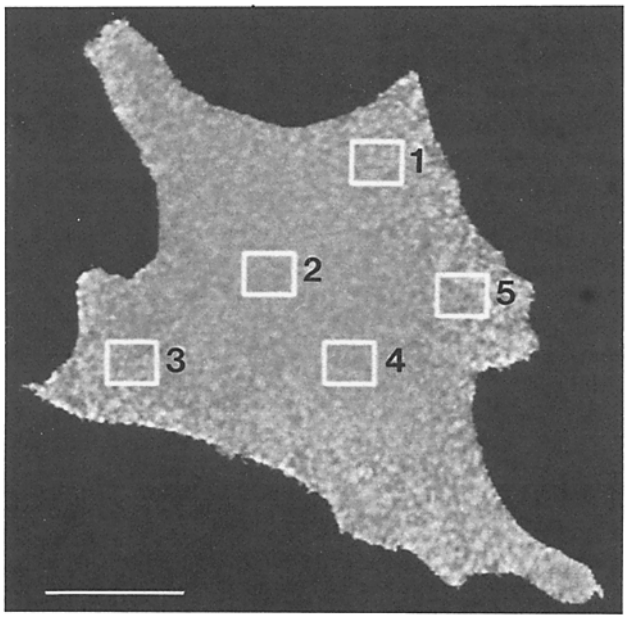

Figure 11. Analysis of subcellular regions. The mean ratio within the region (20 × 20 pixels) of the cytoplasm is relatively constant, even though the CV increases near the edge of the cell. (*1*) Mean = 1.30, CV = 0.09; (*2*) mean = 1.28, CV = 0.05; (*3*) mean = 1.30, CV = 0.10; (*4*) mean = 1.28, CV = 0.06; (*5*) mean = 1.32, CV = 0.13. Bar, 9 μm.

perimposed upon the variations in S/N. Fig. 10 *b* shows an error map (using 7 × 7 pixel averaging) of a pH-clamped cell indicating that most of the cell exhibits <5% deviation from the mean. The thinner peripheral edges exhibit 5–10% (grey) and >10% error (white). The thin white border around the edges of the error map is due to the filtering process. At the edges, the filter averages pixels inside with pixels outside the cell resulting in abnormally low mean values in those regions. Thus, these areas vary significantly from the mean value determined inside the cell so they are depicted only as a border line. Fig. 10 *d* is an error map of the same cell before clamping the pH. Changes in cell shape resulting from cell volume changes complicate a point for point comparison of the error maps. However, more global comparisons are possible. The error at the periphery of the nonclamped cell is most readily explained by the lower S/N in this thin region of the cell. We have not yet detected a reproducible spatial variation in the ratio that cannot be explained simply by a variation in the S/N.

Fig. 11 illustrates the use of the system to measure the pH in different regions (20 × 20 pixel arrays, 29.8 μm^2) of the cell. The near constancy of the mean ratio in different regions of pH-clamped cells demonstrates that the variable pathlength and density of light-scattering particles in cells do not play significant roles in the ratio value. However, the variance of the values increases in the thin periphery due to the weaker signal. An initial analysis of several nonclamped cells in the presence of serum has shown little, if any, spatial variation in cytoplasmic pH. A more detailed spatial analysis of cellular pH will be reported elsewhere.

Table I. Comparison of Cytoplasmic pH in Quiescent and Nonquiescent Swiss 3T3 Cells

Probe	Cell type	Raw ratio	pH* (SEM)	*n*
BCECF	Quiescent	‡	7.09 (0.01)	158
	Nonquiescent	‡	7.35 (0.01)	136
FD	Quiescent	1.57	§	66
	Nonquiescent	1.64	§	76

* Determined from in situ standard curves.
‡ The total data set was measured over several months. Multiple standard curves recorded within 2 wk of given set of data were used. Ratios are therefore not directly comparable.
§ This data subset was derived from experiments performed within a 2-wk period suitable for direct comparison of the ratios. The data are outside the usable range of the in situ standard curve.

Average Cytoplasmic pH of Serum-starved and Nonstarved Cells

Measurement of the cytoplasmic pH in serum-starved and nonstarved Swiss 3T3 cells over a period of months resulted in remarkable consistency. Typically, 10–25 of each type of cell, starved and nonstarved, were measured along with 10 cells pH-clamped with nigericin on each day. The pH-clamped cells provided a means of confirming the consistent and reliable operation of the ratio imaging system. Table I summarizes the data of this study using single cell ratio imaging.

The data indicated a very significant difference (0.25 pH units) between serum-starved and nonstarved cells. Only BCECF, due to its pKa, could be used to measure cytoplasmic pH in these cells. Both probes, however, demonstrated a difference between the quiescent and nonquiescent cells. Fig. 12 shows that there is a greater heterogeneity in cytoplasmic pH in serum-starved cells than nonstarved cells. The population distribution of starved cells is broader and appears to deviate to a greater extent from a normal distribution.

Discussion

Fluorescence Ratio Imaging Microscopy

The validation of fluorescence ratio imaging microscope systems must be demonstrated since factors ranging from lamp characteristics, optics, camera performance, and approaches to image analysis could effect the precision of the measurements. The data in Figs. 1–4 and Fig. 8 critically demonstrate that the present system can be used to quantify ratio measurements in single cells with a high degree of precision. The use of the ratio technique with a properly characterized camera and a stable lamp normalizes the data for pathlength, probe concentration, illumination intensity, and photobleaching over a wide range. Fluorescence ratio imaging microscopy should become more powerful in the future with improvements in probes and instrumentation.

A fundamental requirement for measuring physiological parameters in living cells is the ability to maintain the cells in a physiological environment during the analysis. There is already evidence that strict environmental regulation is required for meaningful measurements of cytoplasmic pH. Moolenaar et al. (46) reported a difference of 0.13 pH units

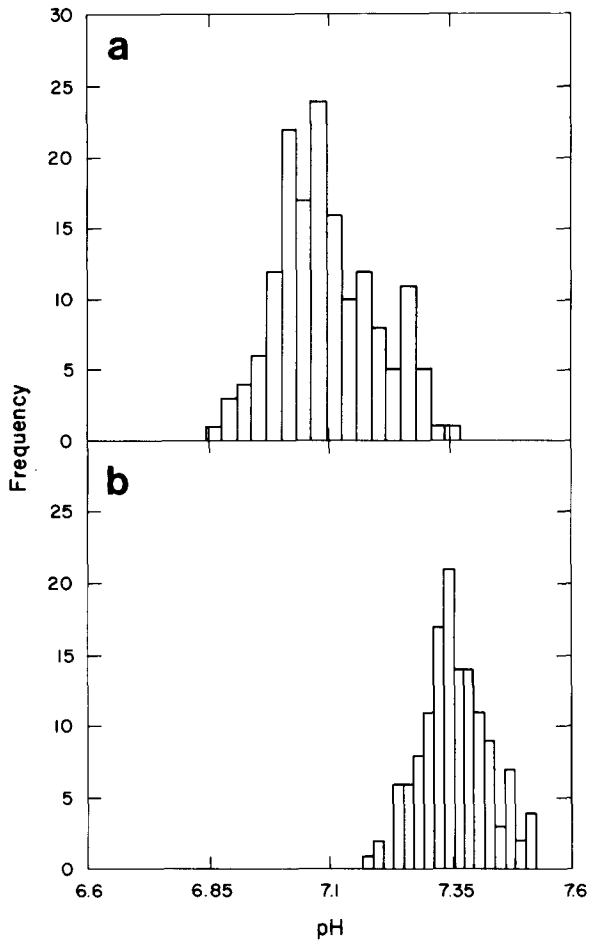

Figure 12. Cell population distribution of cytoplasmic pH. The frequency distribution of mean cytoplasmic pH values for both populations is unimodal with the following characteristics: quiescent cells (*a*), n = 158, mean = 7.09, median = 7.08, SD = 0.10, range = 0.50; nonquiescent cells (*b*), n = 136, mean = 7.35, median = 7.35, SD = 0.07, range = 0.33.

between experiments measured at 20°C and 31°C. Rothenberg et al. (64) and Cassel et al. (11) demonstrated an effect of external medium pH on cytoplasmic pH and Cassel et al. (11) suggested that alkalinization of serum-starved cells might not occur in the presence of bicarbonate buffer. The cell chamber described in this report allows the maintenance of a monitored physiological environment in the absence of organic buffers. Therefore, long term physiological measurements are feasible.

Characteristics of Probes for pH

A variety of probes for cellular pH have been investigated over the last decade (see 51, 61). The sensitivity of fluorescence has encouraged the use of fluorescent probes for pH (12, 21, 22, 25–27, 34, 39, 48–50, 52, 60, 64, 69, 74, 75, 78–81, 88). Recent studies (20, 22, 50) have compared the characteristics of several fluorescent pH sensitive probes in nonimaging applications. The most valuable fluorescent pH indicators fall into two major categories. (*a*) probes that diffuse into cells and are then trapped inside due to cleavage of the probe by cellular esterases (i.e., acetoxymethyl ester forms: 34, 48, 60, 68, 78, 80); and (*b*) probes that must be loaded into cells due to their highly charged nature or due to the presence of a carrier macromolecule (i.e., 25, 64, 69). Recently, criteria for selecting fluorescence indicators of physiological parameters have been suggested (72).

In the present study, we have used FD and BCECF-AM to compare some of the characteristics of these two classes of probes. Swiss 3T3 cells scrape loaded with FD and allowed to spread in medium containing serum exhibited normal physiology (43). Very few fluorescent vesicles were observed and the cells exhibited normal behavior for several cell divisions. The FD also remained trapped in the cytoplasm as evidenced by the absence of an immobile fraction in FRAP experiments and the detection of probe exclusion from organelles such as nuclei, mitochondria, and endosomes. Serum-starved cells exhibited numerous vesicles presumably due to enhanced autophagocytosis due to starvation (23). The disadvantages of using a carrier molecule include the need for a loading procedure such as direct microinjection or a population loading procedure (43, 64) and a wide range of loading efficiencies. Unfortunately, the pKa of FD is not in the range for quantitation of the cytoplasmic pH of these cells, but can be used to monitor the pH of more acidic compartments such as endosomes.

The advantages of the diffusible/cleavable probes include the simplicity of labeling large numbers of cells with relative uniformity. Swiss 3T3 cells labeled with low concentrations of BCECF-AM for long incubation times exhibited the least toxic response. The probe entered the nucleus and penetrated to the very edge of the cell. The hydrolyzed dye was relatively mobile in the cytoplasm based on the FRAP assay. The disadvantages include the lack of complete specificity of labeling just cytoplasm while avoiding other cellular compartments, the slow leakage of the probe out of the cell, and the potential toxic effects of the by-products of acetoxymethyl ester hydrolysis (see 74).

Unlike cells loaded with FD, cells labeled with BCECF-AM exhibited obvious toxic effects ~2.5 h postlabeling. Therefore, our experiments were limited to a narrow time period. The serum-starved cells exhibited the same basic characteristics, but required a much shorter time for labeling due to an apparent higher esterase content and/or activity. BCECF-AM cannot be used for long term cell investigations under the conditions used in this study. Our results indicate that a neutral carrier, such as dextran, might be necessary for long term studies (64, 69). We are currently testing BCECF coupled to different sizes of dextrans.

Spatial Measurements by Fluorescence Ratio Imaging Microscopy

The reason for using an imaging approach is to map the spatial, as well as the temporal, dynamics of specific molecules and ions during cellular processes (see 72). Measurements on cell suspensions or cell populations plated onto coverslips in a fluorometer are valuable for obtaining an average value for a population response. Flow cytometry can measure variations on a cell by cell basis and therefore give a population distribution. However, kinetic information is necessarily a population average since each cell is measured only once. Furthermore, flow cytometry also can only be used with cell

suspensions. Microspectrofluorometry, using a photomultiplier or comparable detector, allows the measurement of both population averages using low magnification and single cell kinetics using high magnification. The spatial information is limited since only one subcellular region can be monitored at a time. However, the temporal resolution is maximized within this region. The imaging approach complements these other methods and permits the measurement of responses from single cells, simultaneous responses from multiple subcellular compartments, as well as population distributions.

Fluorescence imaging microscopy offers distinct advantages over other methods of measuring fluorescence signals. (*a*) Single cell spatial kinetic information is available using high magnification. Multiple cells can be monitored within the same experiment with the computer-controlled stage. However, the number of cells per experiment is limited by the kinetics of the process being monitored and the speed of the scanning stage. (*b*) Low magnification allows single cell kinetics to be monitored with lower spatial information on large numbers of cells in a single field. Multiple fields increase the total number of cells that can be analyzed in a single experiment. (*c*) The imaging approach allows debris, which may be labeled nonspecifically, to be removed either by selecting fields that do not have such artifacts or by removing them during the image analysis stage. (*d*) The imaging approach also allows the selection of particular types of cells for analysis (e.g., flat cells, round cells, dividing cells, etc.). Thus, a single cell analysis allows the collection and classification of individual cell types. In addition, the ability to spectrally resolve multiple fluorescent probes allows the computer-controlled microscope to monitor multiple specific parameters within the same cell. The fluorescence imaging microscope provides the necessary instrumentation for correlating multiple physiological parameters within living cells (6, 72, 82).

It must be recognized that the ratio imaging approach has some limitations as currently practiced, although precise measurements are possible and accurate measurements depend upon the accuracy of the standard curves. The time resolution of measurements is limited by the S/N. The use of low irradiance at the specimen plane to minimize photobleaching results in the need to average multiple images. Therefore, a single measurement can require several seconds for completion. Rapid and transient changes in parameters such as pH or pCa still require the use of fast response-time photomultipliers/array detectors with the loss of spatial information. In addition, the spatial S/N ratio (69) ultimately limits the spatial domains that can be quantified (Figs. 8–11). Therefore, a combination of imaging and photometric measurements should provide the spatial and temporal information required in a particular experiment.

The spatial S/N of any fluorescence imaging microscope must be defined before attempting to measure spatial variations of physiological parameters. Our present system has a practical spatial resolution of 3.65 μm^2, since that area (7 $\times$ 7 pixels) must be averaged to keep the CV <3% in a solution model (Fig. 8). Measurements of spatial information in living cells are complicated by two additional significant factors: (*a*) the thinner regions of the cells, such as the periphery, exhibit lower S/N as compared with the thicker central regions (Fig. 10); and (*b*) active cellular movements can cause a loss of registration between Im^{489} and Im^{452} (see Figs. 6 and 7 *b*). Therefore, measurements of pH in thin, motile regions of cells are difficult. However, advances in illumination and detection systems should overcome these limitations.

We can make several generalizations based on our current data. Measurements of cytoplasmic pH indicate little, if any, spatial variation in cells in the presence of serum (Fig. 11) or after 24-h starvation. Furthermore, there is no discernible difference between the cytoplasmic pH and nuclear pH in Swiss 3T3 cells in contrast to the report describing differences of pCa in the nucleus vs. cytoplasm of smooth muscle cells (86).

Cytoplasmic pH in Quiescent and Nonquiescent Swiss 3T3 Cells

The possible role of cytoplasmic alkalinization in the se-

Table II. Comparison of Cytoplasmic pH of Fibroblasts Using Different Methods

Probe	Method	Cell type	pH (SEM)	Reference
DMO	Radiolabel	Quiescent Sw3T3 Nonquiescent Sw3T3	7.21 (0.07) 7.36 (0.09)	Schuldiner and Rozengurt, 1982
DMFD	Fluorescence intensity	Quiescent NR6* Stimulated NR6	6.90 (0.05)‡ 7.04§	Cassel et al., 1983
Benzoic acid	Radiolabel	Quiescent CHL Nonquiescent CHL	7.39 (0.01) 7.49 (0.01)	L'Allemain et al., 1984
BCECF	Fluorescence intensity	Quiescent HF Stimulated HF	7.05 (0.02) 7.26	Moolenaar et al., 1984
BCECF	Fluorescence intensity	Quiescent Sw3T3 Nonquiescent Sw3T3	7.01 (0.03) 7.14 (0.03)	Hesketh et al., 1985
BCECF	Single cell ratio imaging	Quiescent Sw3T3 Nonquiescent Sw3T3	7.09 (0.01) 7.35 (0.01)	This study

Abbreviations: DMO, 5.5-dimethyl-2.4-oxazolidinedione; DMFD, dimethyl carboxyfluorescein dextran; Sw3T3, Swiss 3T3; HF, human foreskin fibroblast; CHL, Chinese hamster lung fibroblast.
* Cell line derived from mouse 3T3.
‡ SD.
§ Value calculated from reported increase in pH upon stimulation by serum. A transiently higher pH is followed by stabilization at 0.1 pH units above initial pH.

quence of cellular responses to growth factor stimulation has stimulated a great deal of effort in quantifying cytoplasmic pH in serum-starved and serum- or growth factor–stimulated cells (for a review see 48 and 44). From the fact that cytoplasmic pH has a dramatic effect on the total cellular chemistry ranging from pCa (8), metabolism (19, 76), protein synthesis (87), and potential cell motility (15, 17, 58), it is imperative that a precise and accurate measure of this fundamental physiological parameter be established.

The present study has demonstrated a difference in the cytoplasmic pH between serum-starved cells and cells maintained in serum in the presence of bicarbonate buffer. Cells maintained in serum exhibited a mean cytoplasmic pH of 7.35, whereas serum-starved cells had a mean pH of 7.1. Studies on >130 cells under each condition indicated only a relatively small variation among cells (Table I, Fig. 12). Table II compares our data with data from other laboratories using a variety of methods. Most of the fluorescent probe methods are in rather close agreement and give lower pH values than the methods using the distribution of weak acids. This might be explained by the ineffective accounting of the more basic mitochondrial compartment that is accessible to the weak acid distribution approach (see 61, 62). The mean cytoplasmic pH for both serum-starved and nonstarved cells (Fig. 12) demonstrates the presence of a unimodal distribution of cells under each condition. This point is important since previous studies have been based on population averaging techniques, which give no information about subpopulation distributions. Our results also demonstrate the absence of an obvious spatial variation in cytoplasmic pH in the two states.

The validation of the fluorescence ratio imaging system, the demonstration of the maintenance of a physiological environment, and the characterization of the limits of the pH probes make it possible to investigate the temporal and spatial dynamics of cytoplasmic pH and other physiological parameters under a variety of experimental conditions, including cell stimulation with growth factors. The question of cytoplasmic alkalinization can now be investigated on a cell by cell basis under physiological conditions based on this baseline study. It is clear from the present results that serum-starved cells are more acidic than cells maintained in serum. Therefore, a critical issue is whether any increase in cytoplasmic pH upon stimulation can really be defined as an alkalinization or a return to the normal cytoplasmic pH. Interestingly, the $[Ca^{++}]_i$ of serum-starved Swiss 3T3 cells has been reported as 89 ± 20 μM, while cells maintained in serum exhibited a $[Ca^{++}]_i$ of 50 ± 19 μM (42). It will be important to quantify both the temporal and spatial variations of cytoplasmic pH and pCa in the same cells in future studies, along with other biochemical properties of cells. The use of mutants exhibiting altered ion transport (56), as well as inhibitors of specific ion exchangers (5, 28, 35, 48, 64, 66) in conjunction with single cell analysis, will continue to be valuable in dissecting the mechanisms involved in regulating cytoplasmic pH.

We wish to thank Robbin DeBiasio for her expert technical assistance with cell culture and Albert Gough and Dr. Kate Luby-Phelps for assistance with FRAP. We thank Drs. Lerson Tanasugarn, Kendal Preston, Fred Lanni, and Jesse Sisken for many helpful discussions. We thank also Drs. Fred Lanni, Jesse Sisken, and Len Pagliaro for critically reading the manuscript.

This work has been supported by grants from the National Institutes of Health (NIH) (AM-32461), NIH Program Project (1-POI-GM-34639), National Science Foundation (DMB-8414772), and the Council for Tobacco Research, USA, Inc. (1412a) to D. L. Taylor. G. R. Bright has been supported by a Leukemia Society Postdoctoral Fellowship and G. W. Fisher has been supported by a NIH Postdoctoral Fellowship (AI-07266).

Received for publication 13 October 1986, and in revised form 8 December 1986.

References

1. Agard, D. A., and J. W. Sedat. 1983. Three-dimensional architecture of a polytene nucleus. *Nature (Lond.).* 302:676–681.
2. Arndt-Jovin, D. J., M. Robert-Nicoud, S. J. Kaufman, and T. M. Jovin. 1985. Fluorescence digital imaging microscopy (DIM) in cell biology. *Science (Wash. DC).* 230:247–256.
3. Barrows, G. H., J. E. Sisken, J. C. Allegra, and S. D. Grasch. 1984. Measurement of fluorescence using digital integration of video images. *J. Histochem. Cytochem.* 32:741–746.
4. Benson, D. M., J. Bryan, A. L. Plant, A. M. Gotto, Jr., and L. C. Smith. 1985. Digital imaging fluorescence microscopy: spatial heterogeneity of photobleaching rate constants in individual cells. *J. Cell. Biol.* 100:1209–1323.
5. Boron, W. F. 1983. Transport of H^+ and of ionic weak acids and bases. *J. Membr. Biol.* 72:1–16.
6. Bright, G. R., and D. L. Taylor. 1986. Imaging at low light level in fluorescence microscopy. *In* Applications of Fluorescence in the Biomedical Sciences. D. L. Taylor, A. S. Waggoner, R. F. Murphy, F. Lanni, and R. R. Birge, editors. Alan R. Liss, Inc., New York. 257–288.
7. Busa, W. B. 1986. Mechanisms and consequences of pH-mediated cell regulation. *Ann. Rev. Physiol.* 48:389–402.
8. Busa, W. B., and R. Nuccitelli. 1984. Metabolic regulation via intracellular pH. *Am. J. Physiol.* 246:R409–R438.
9. Caspersson, T. 1950. Über die Rolle der desoxyribosenukleinsaure bei der Zellteilung. *Chromosoma (Berl.).* 1:147–156.
10. Cassel, D., P. Rothenberg, Y. X. Zhuang, T. F. Deuel, and L. Glaser. 1983. Platelet-derived growth factor stimulates Na^+/H^+ exchange and induces cytoplasmic alkalinization in NR6 cells. *Proc. Natl. Acad. Sci. USA.* 80:6224–6228.
11. Cassel, D., B. Whiteley, Y. X. Zhuang, and L. Glaser. 1985. Mitogen-independent activation of Na^+/H^+ exchange in human epidermal carcinoma A431 cells: regulation by medium osmolarity. *J. Cell Physiol.* 122:178–186.
12. Chaillet, J. R., K. Amsler, and W. F. Boron. 1986. Optical measurements of intracellular pH in single LLC-PK1 cells: demonstration of $Cl\text{-}HCO_3$ exchange. *Proc. Natl. Acad. Sci. USA.* 83:522–526.
13. Chance, B. 1963. Localization of intracellular and intramitochondrial compartments. *Ann. NY Acad. Sci.* 108:322–330.
14. Chance, B., and B. Thorell. 1959. Localization and kinetics of reduced pyridine nucleotides in living cells by microfluorometry. *J. Biol. Chem.* 234:3044–3050.
15. Condeelis, J., and D. L. Taylor. 1977. The contractile basis of amoeboid movement. V. The control of gelation, solation, and contraction in extracts of *Dictyostelium discoideum. J. Cell Biol.* 74:901–927.
16. Fay, F., K. Fogarty, and J. Coggins. 1986. The analysis of molecular distribution in single cells using a digital imaging microscope. *Soc. Gen. Physiol. Ser.* 40:51–64.
17. Fechheimer, M., J. Brier, M. Rockwell, E. Luna, and D. L. Taylor. 1982. A calcium and pH regulated actin binding protein from *D. discoideum. J. Cell Motility.* 2:289–308.
18. Fechheimer, M., C. Denny, R. Murphy, and D. L. Taylor. 1986. Measurement of cytoplasmic pH in *D. discoideum* using a new method for introducing macromolecules into cells. *Eur. J. Cell Biol.* 40:242–247.
19. Fidelman, M. L., S. H. Seeholzer, K. B. Walsh, and R. D. Moore. 1982. Intracellular pH mediates action of insulin on glycolysis in frog skeletal muscle. *Am. J. Physiol.* 242:C87–C93.
20. Geisow, M. J. 1984. Fluorescein conjugates as indicators of subcellular pH. A critical evaluation. *Exp. Cell Res.* 150:29–35.
21. Geisow, M. J., and W. H. Evans. 1984. pH in the endosome. Measurements during pinocytosis and receptor-mediated endocytosis. *Exp. Cell Res.* 150:36–46.
22. Graber, M. L., D. C. DiLillo, B. L. Friedman, and E. Pastoriza-Munoz. 1986. Characteristics of fluoroprobes for measuring intracellular pH. *Anal. Biochem.* 156:202–212.
23. Gronostajski, R. M., A. L. Goldberg, and A. B. Pardee. 1984. The role of increased proteolysis in the atrophy and arrest of proliferation in serum-deprived fibroblasts. *J. Cell. Physiol.* 121:189–198.
24. Grynkiewicz, G., M. Poenie, and R. Y. Tsien. 1985. A new generation of Ca^{2+} indicators with greatly improved fluorescence properties. *J. Biol. Chem.* 260:3440–3450.
25. Heiple, J., and D. L. Taylor. 1980. Intracellular pH in single motile cells. *J. Cell Biol.* 88:885–890.
26. Heiple, J., and D. L. Taylor. 1982. pH changes in the pinosomes and

phagosomes in the amoeba, *Chaos carolinenses*. *J. Cell Biol.* 94:143–149.
27. Heiple, J., and D. L. Taylor. 1982. An optical technique for measurement of intracellular pH in single living cells. *In* Intracellular pH: Its Measurements, Regulation, and Utilization in Cellular Functions. R. Nuccitelli and D. W. Deamer, editors. Alan R. Liss Inc., New York. 22–54.
28. Hesketh, T. R., J. P. Moore, J. D. H. Morris, M. V. Taylor, J. Rogers, G. A. Smith, and J. C. Metcalfe. 1985. A common sequence of calcium and pH signals in mitogenic stimulation of eukaryotic cells. *Nature (Lond.)*. 313:481–484.
29. Kapitza, H. G., G. McGregor, and K. A. Jacobson. 1985. Direct measurement of lateral transport in membranes by using time-resolved spatial photometry. *Proc. Natl. Acad. Sci. USA*. 83:4122–4126.
30. Keith, C. H., B. Ratan, F. R. Maxfield, A. Bajer, and M. L. Shelanski. 1985. Local cytoplasmic calcium gradients in living mitotic cells. *Nature (Lond.)*. 316:848–850.
31. Kohen, E., J. G. Hirschberg, C. Kohen, A. Wouters, H. Pearson, J. M. Salmon, and B. Thorell. 1975. Multichannel microspectrofluorometry for topographic and spectral analysis of NAD(P)H fluorescence in single living cells. *Biochim. Biophys. Acta*. 396:149–154.
32. Kohen, E., B. Thorell, J. G. Hirschberg, A. W. Wouters, C. Kohen, P. Bartick, J.-M. Salmon, P. Viallet, D. O. Schachtschabel, A. Rabinvitch, D. Mintz, P. Meda, H. Westeroff, J. Nestor, and J. S. Ploem. 1981. Microfluorometric procedures and their applications in biological systems. *In* Modern Fluorescence Spectroscopy. Vol. 3. E. L. Wehry, editor. Plenum Publishing Corp., New York. 295–346.
33. Kruskal, B. A., S. Shak, and F. R. Maxfield. 1986. Spreading of human neutrophils is immediately preceded by a large increase in cytoplasmic free calcium. *Proc. Natl. Acad. Sci. USA*. 83:2919–2923.
34. Kurtz, I., and R. S. Balaban. 1985. Fluorescence emission spectroscopy of 1.4-dihydroxyphthalonitrile. A method of determining intracellular pH in cultured cells. *Biophys. J.* 48:499–508.
35. L'Allemain, G., S. Paris, and J. Pouyssegur. 1984. Growth factor action and intracellular pH regulation in fibroblasts. *J. Biol. Chem.* 259:5809–5815.
36. Lanni, F. 1986. New aspects of microscopy in cell biology. *In* Applications of Fluorescence in the Biomedical Sciences. D. L. Taylor, A. S. Waggoner, R. F. Murphy, F. Lanni, and R. R. Birge, editors. Alan R. Liss Inc., New York. 449–460.
37. Luby-Phelps, K., F. Lanni, and D. L. Taylor. 1985. Behavior of a fluorescent analog of calmodulin in living 3T3 cells. *J. Cell Biol.* 101:1245–1256.
38. Luby-Phelps, K., D. L. Taylor, and F. Lanni. 1986. Probing the structure of cytoplasm. *J. Cell Biol.* 102:2015–2022.
39. MacDonald, V., J. Keiger, and F. Jobsis. 1977. Spectrophotometric measurements of metabolically induced pH changes in skeletal muscle. *Arch. Biochem. Biophys.* 184:423–430.
40. McNeil, P., and D. L. Taylor. 1986. Early cytoplasmic signals and cytoskeletal responses initiated by growth factors in cultured cells. *In* Cell Membranes: Methods and Reviews. E. Elson, W. Frazier, and L. Glaser, editors. Plenum Publishing Corp., New York. In press.
41. McNeil, P., L. Tanasugarn, J. Meigs, and D. L. Taylor. 1983. Acidification of phagosomes is initiated before lysosomal enzyme activity is detected. *J. Cell Biol.* 97:692–702.
42. McNeil, P., M. McKenna, and D. L. Taylor. 1985. A transient rise in cytosolic calcium follows stimulation of quiescent cells with growth factors and is inhibitable with phorbol myristate acetate. *J. Cell Biol.* 101:372–379.
43. McNeil, P. L., R. F. Murphy, F. Lanni, and D. L. Taylor. 1984. A method for incorporating macromolecules into adherent cells. *J. Cell Biol.* 98: 1556–1564.
44. McNeil, P., J. Swanson, S. Wright, S. Silverstein, and D. L. Taylor. 1986. Fc-receptor-mediated phagocytosis occurs in macrophages without an increase in average $[Ca^{++}]$. *J. Cell Biol.* 102:1586–1592.
45. Moolenaar, W. H. 1986. Effects of growth factors on intracellular pH regulation. *Ann. Rev. Physiol.* 48:363–376.
46. Moolenaar, W. H., L. G. J. Tertoolen, and S. W. de Laat. 1984. The regulation of cytoplasmic pH in human fibroblasts. *J. Biol. Chem.* 259:7563–7570.
47. Moolenaar, W. H., L. G. J. Tertoolen, and S. W. de Laat, 1984. Growth factors immediately raise cytoplasmic free Ca^{2+}. *J. Biol. Chem.* 259: 8066–8069.
48. Moolenaar, W. H., R. Y. Tsien, P. T. van der Saag, and S. W. de Laat. 1983. Na^+/H^+ exchange and cytoplasmic pH in the action of growth factors in human fibroblasts. *Nature (Lond.)*. 304:645–648.
49. Murphy, R. F., S. Powers, and C. R. Cantor. 1984. Endosome pH measured in single cells by dual fluorescence flow cytometry: rapid acidification of insulin to pH 6. *J. Cell Biol.* 98:1757–1762.
50. Musgrove, E., C. Rugg, and D. Hedley. 1986. Flow cytometric measurement of cytoplasmic pH: a critical evaluation of available fluorochromes. *Cytometry*. 7:347–355.
51. Nuccitelli, R., and D. W. Deamer. 1982. Intracellular pH: Its Measurement, Regulation, and Utilization in Cellular Function. Alan R. Liss Inc., New York.
52. Ohkuma, S., and B. Poole. 1978. Fluorescence probe measurement of the intralysomal pH in living cells and the perturbation of pH by various agents. *Proc. Natl. Acad. Sci. USA*. 75:3327–3331.
53. Ploem, J. S. 1986. New instrumentation for sensitive image analysis of fluorescence in cells and tissues. *In* Applications of Fluorescence in the Biomedical Sciences. D. L. Taylor, A. S. Waggoner, R. F. Murphy, F. Lanni, and R. R. Birge, editors. Alan R. Liss, Inc., New York. 289–300.
54. Poenie, M., J. Alderton, R. Steinhardt, and R. Tsien. 1986. Calcium rises abruptly and briefly throughout the cell at the onset of anaphase. *Science (Wash. DC)*. 233:886–889.
55. Pollister, A. W., and H. Ris. 1947. Nucleoprotein determinations in cytological preparations. *Cold Spring Harbor Symp. Quant. Biol.* 12:147–157.
56. Pouyssegar, J., C. Sardet, A. Franchi, G. L'Allemain, and S. Paris. 1984. A specific mutation abolishing Na^+/H^+ antiport activity in hamster fibroblasts precludes growth at neutral and acidic pH. *Proc. Natl. Acad. Sci. USA*. 81:4833–4837.
57. Ratan, R. R., M. L. Shelanski, and F. R. Maxfield. 1986. Transition from metaphase to anaphase is accompanied by local changes in cytoplasmic free calcium in PtK2 kidney epithelium cells. *Proc. Natl. Acad. Sci. USA*. 83:5136–5140.
58. Regula, C., J. Pfeiffer, and R. Berlin. 1981. Microtubule assembly and disassembly at alkaline pH. *J. Cell Biol.* 89:45–53.
59. Reynolds, G. T., and D. L. Taylor. 1980. Image intensification applied to light microscopy. *Bioscience*. 30:586–592.
60. Rink, T. J., R. Y. Tsien, and T. Pozzan. 1982. Cytoplasmic pH and free Mg^{2+} in lymphocytes. *J. Cell Biol.* 95:189–196.
61. Roos, A., and W. F. Boron. 1981. Intracellular pH. *Physiol. Rev.* 61:296–434.
62. Roos, A., and D. W. Keifer. 1982. Estimation of intracellular pH from the distribution of weak electrocytes. *In* Intracellular pH: Its Measurement, Regulation, and Utilization in Cellular Function. R. Nuccitelli and D. W. Deamer, editors. Alan R. Liss Inc., New York.
63. Rost, F. 1971. A microspectrofluorometer for measuring spectra of excitation emission and absorption in cells and tissues. *In* Fluorescence Techniques in Cell Biology. A Thaer and M. Sernetz, editors. Springer-Verlag, Berlin. 57–63.
64. Rothenberg, P., L. Glaser, P. Schlesinger, and D. Cassel. 1983. Activation of Na^+/H^+ exchange by epidermal growth factor elevates intracellular pH in A431 cells. *J. Biol. Chem.* 258:12644–12653.
65. Sawyer, D. W., J. A. Sullivan, and G. L. Mandel. 1985. Intracellular free calcium localization in neutrophils during phagocytosis. *Science (Wash. DC)*. 230:663–666.
66. Schuldiner, S., and E. Rozengurt. 1982. Na^+/H^+ antiport in Swiss 3T3 cells: mitogenic stimulation leads to cytoplasmic alkalinization. *Proc. Natl. Acad. Sci. USA*. 79:7778–7782.
67. Seliger, H. H., and W. D. McElroy. 1965. Light: Physical and Biological Action. Academic Press Inc., New York.
68. Simons, E. R., D. B. Schwartz, and N. E. Norman. 1982. Stimulus response coupling in human platelets: trombin-induced changes in pH_i. *In* Intracellular pH: Its Measurement, Regulation, and Utilization in Cellular Function. R. Nuccitelli and D. W. Deamer, editors. Alan R. Liss Inc., New York. 463–482.
69. Tanasugarn, L., P. McNeil, G. Reynolds, and D. L. Taylor. 1984. Microspectrofluorometry by digital image processing: measurement of cytoplasmic pH. *J. Cell Biol.* 98:717–724.
70. Taylor, D. L., and Y. L. Wang. 1980. Fluorescently labeled molecules as probes of the structure and function of living cells. *Nature (Lond.)*. 284: 405–410.
71. Taylor, D. L., P. A. Amato, K. Luby-Phelps, and P. McNeil. 1984. Fluorescent analog cytochemistry. *Trends in Biochem. Sci.* 9:88–89.
72. Taylor, D. L., P. A. Amato, P. L. McNeil, K. Luby-Phelps, and L. Tanasugarn. 1986. Spatial and temporal dynamics of specific molecules and ions in living cells. *In* Applications of Fluorescence in the Biomedical Sciences. D. L. Taylor, A. S. Waggoner, R. F. Murphy, F. Lanni, and R. R. Birge, editors. Alan R. Liss Inc., New York. 347–376.
73. Thaer, A., and M. Sernetz. 1973. Fluorescence Techniques in Cell Biology. Springer-Verlag New York, Inc.
74. Thomas, J. A. 1986. Intracellularly trapped pH indicators. *Soc. Gen. Physiol. Ser.* 40:311–325.
75. Thomas, J. A., R. M. Buchsbaum, A. Zimniak, and E. Racker. 1979. Intracellular pH measurements in Ehrlich ascites tumor cells utilizing spectroscopic probes generated in situ. *Biochemistry*. 18:2210–2218.
76. Triveda, B., and W. H. Danforth. 1966. Effect of pH on the kinetics of muscle phosphofructokinase. *J. Biol. Chem.* 241:4110–4114.
77. Tsien, R. Y., T. Pozzan, and T. J. Rink. 1982. Calcium homeostasis in intact lymphocytes: cytoplasmic free calcium monitored with a new, intracellularly trapped fluorescent indicator. *J. Cell Biol.* 94:325–334.
78. Tycko, B., and F. Maxfield. 1982. Rapid acidification of endocytic vesicles containing alpha-2-macroglobulin. *Cell*. 28:643–651.
79. Tycko, B., C. H. Keith, and F. R. Maxfield. 1983. Rapid acidification of endocytic vesicles containing asialoglycoprotein in cells of a human hepatoma line. *J. Cell Biol.* 97:1762–1776.
80. Valet, G., A. Raffael, L. Moroder, E. Wunsch, and G. Ruhenstroth-Bauer. 1981. Fast intracellular pH determination in single cells by flow cytometry. *Naturwissenschaften*. 68:265–266.

81. Visser, J. W. M., A. A. M. Jongeling, and H. J. Tanke. 1979. Intracellular pH-determination by fluorescence measurements. *J. Histochem. Cytochem.* 27:32–35.
82. Waggoner, A. S. 1986. Fluorescent probes for analysis of cell structure, function, and health by flow cytometry and imaging cytometry. *In* Applications of Fluorescence in the Biomedical Sciences. D. L. Taylor, A. S. Waggoner, R. F. Murphy, F. Lanni, and R. R. Birge, editors. Alan R. Liss Inc., New York. 3–28.
83. Wampler, J. E. 1986. Instrumentation: seeing the light and measuring it. *In* Chemiluminescence and Bioluminescence. J. Burr, editor. Marcel Dekker Inc., New York. 1–44.
84. Webb, W. W., and D. Gross. 1986. Patterns of individual molecular motions deduced from fluorescent image analysis. *In* Applications of Fluorescence in the Biomedical Sciences. D. L. Taylor, A. S. Waggoner, R. F. Murphy, F. Lanni, and R. R. Birge, editors. Alan R. Liss, Inc., New York. 405–422.
85. West, S. S. 1969. Fluorescence microspectrophotometry of supravitally stained cells. *In* Physical Techniques in Biological Research. Vol. 3C, Cells and Tissues. A. W. Pollister, editor. Academic Press Inc., New York. 253–321.
86. Williams, D. A., K. E. Fogarty, R. Y. Tsien, and F. S. Fay. 1985. Calcium gradients in single smooth muscle cells revealed by the digital imaging microscope using Fura-2. *Nature (Lond.).* 318:558–561.
87. Winkler, M. M., R. A. Steinhardt, J. L. Grainger, and L. Minning. 1980. Dual ionic controls for the activation of protein synthesis at fertilization. *Nature (Lond.).* 287:558–560.
88. Wolfbeis, O. S., E. Furlinger, H. Kroneis, and H. Marsoner. 1983. Fluorometric analysis. 1. A study on fluorescent indicators for measuring near neutral ("physiological") pH-values. *Fresenius Z. Anal. Chem.* 314:119–124.
89. Woodbury, J. W. 1965. The cell membrane: ionic and potential gradients and active transport. *In* Physiology and Biophysics. T. C. Ruch and H. D. Patton, editors. W. B. Saunders Co., Philadelphia. 1–25.